

Sentinel-1 and Sentinel-2 data fusion system for surface water extraction

Mostafa Saghafi, Ahmad Ahmadi, and Behnaz Bigdeli*

Shahrood University of Technology, Department of Civil Engineering, Shahrood, Iran

Abstract. Detecting and monitoring surface water has received much attention in recent decades. Surface water is one of the most critical water resources for both human and ecological systems. Remote sensing technology has made it possible to have accurate and frequent updates of surface water. We propose a remote sensing multisensor fusion system using optical data including Landsat-8 and Sentinel-2 and RADAR data including Sentinel-1 for water body extraction. Using a data fusion approach, the spatial resolution of multispectral images increased from 30 to 10 m, and the spectral information of Landsat-8 and Sentinel-2 were preserved. Then, all features extracted from the high spatial resolution images, water index maps, and Sentinel-1 dataset were combined as a stacked feature space. The new data were subsequently classified by support vector machine, neural network, and random forest. Finally, all classifiers' outputs were integrated using a weighted majority voting decision fusion strategy, which significantly improved surface water extraction. Our study illustrates the ability of remote sensing multisensory fusion, water indices, and decision fusion for water body extraction. © 2021 Society of Photo-Optical Instrumentation Engineers (SPIE) [DOI: 10.1117/1.JRS.15.014521]

Keywords: surface water; remote sensing; water indices; data fusion; decision fusion.

Paper 200587 received Aug. 5, 2020; accepted for publication Mar. 3, 2021; published online Mar. 23, 2021.

1 Introduction

Environmental changes that have a direct impact on natural systems most often caused by human influences and natural ecological processes are one of the most important issues associated with human societies in this decade.^{1–3} As one of the most critical environmental changes, surface water bodies and their changes are important for both human and ecological systems.⁴ Water on the surface of the Earth, such as rivers, lakes, wetlands, and oceans, is called surface water.⁵ Some issues, such as flooding, outbreaks of waterborne disease, and water shortages in dry tropical areas, may change surface water.⁶ Recently, monitoring surface water has been essential for policy and decision-making processes in numerous countries.⁷

Remote sensing plays a vital role in detecting and monitoring the Earth's terrain and providing useful collections of data and information from the Earth's surface and its objects.⁸ Recently, various remote sensing sensors have been applied to identify some characteristics of water bodies on the Earth, such as flood prediction and evaluation of water resources, shoreline change and erosion monitoring, and coastal and zone management, while human life and ecosystems have a direct relationship with them.⁹ Recently, satellite and remote sensing sensors provide useful collections of data and information about objects that provide various temporal scales, with large spatial coverage and low cost, among other benefits.¹⁰ Passive remote sensing sensors [panchromatic, multispectral (MS), or hyperspectral (HS) images] have advantages such as high spatial resolution and low noise and disadvantages such as problems in collecting data at night and in cloudy weather. Also, active remote sensing sensors such as light detection and ranging (Lidar) and RADAR provide complementary information (spectral reflectance and height), which are independent of weather (fog, rain, smoke, and cloud) and sunlight conditions.^{11–13} However, these kinds of sensors have complexities and problems such as speckle noises and advanced pre-processing, as opposed to optical data.^{14–18} Single remote sensing sensors are

*Address all correspondence to Behnaz Bigdeli, bigdeli@shahroodut.ac.ir

unable to provide complete, consistent, or precise data for information extraction from Earth's objects. Recently, multisensor fusion systems that fuse information from multiple sensors have been developed to produce a better understanding and complementary information of observed sites.^{11,19,20}

Some researchers have applied optical remote sensing sensors, such as Landsat-8 Operational Land Imager (OLI) and Sentinel-2, for water body extraction, whereas others have focused on the use of RADAR technologies in this field. However, due to the low accuracy of single sensors, recently, a combination of remote sensing sensors has provided greater improvement in environmental studies.^{5,21,22}

As mentioned, some researchers applied different optical remote sensing data for extracting and monitoring water bodies. Jiang et al.²³ proposed Sentinel-2 water index (SWI) to distinguish the large-scale surface water using the Sentinel-2. They utilized the Otsu method for normalized difference water index (NDWI) and SWI to extract water bodies. The results demonstrated that the SWI index has better performance than the NDWI to classify urban areas, sediment, salt, and ice from the water body. It illustrates that the SWI index can accurately extract water and non-water. However, this index is suitable for large-scale water, and it is not proper for detecting small rivers.²⁴ Ali et al.²⁵ studied the relation between urban development and urban surface water bodies using the Landsat-8 OLI optical satellite. They used water indices such as NDWI and modified normalized difference water index (MNDWI) to categorize water bodies into water and non-water objects and to prepare data for classification. As a result, the low accuracy of detecting the surface water using Landsat-8 with 15 m spatial resolution was improved using water indices that illustrate the water indices' role.²⁵ Acharya et al.²² evaluated the water indices' accuracy using Landsat-8 image data for Nepal. They combined water indices and used an optimum threshold to improve water extraction accuracy. In this method, NDWI and normalized difference vegetation index (NDVI) were combined to form the NDWmVI, and similarly, AWEIshmVI was formed from a combination of automated water extraction index_shadow (AWEI_sh) and NDVI indices. Also, they used elevation data and combined it with NDVI and NDWI to form the Elev_NDWnVI. They found that a combination of NDWI and AWEI_sh with NDVI was unable to improve water detection accuracy. Finally, a combination of elevation with NDVI and NDWI indices significantly improved water detection.²² One of the most important results is the importance of the digital elevation model (DEM) layer in enhancing the identification of surface water using water indices. The elevation layer of the study area caused shadows that sometimes led to water detection being eliminated with the use of an optimum thresholding approach. The results, using only one optical sensor, showed that the combination of water indices with the elevation layer performed an influential role in increasing the accuracy of surface water identification. Xiong et al.¹⁰ developed a new subpixel surface water extraction (SSWE) to extract surface water using Landsat-8 OLI images. In this investigation, three approaches were used for SSWE. First, for pure water extraction, all-band water index (ABWI) was used; second, mix-water lands were extracted with the morphological dilation approach; and finally, water fractions within the mixed water–land pixels were estimated by multiple endmember spectral mixture analysis. The SSWE method extracts surface water bodies in complex aquatic environments areas with high accuracy.¹⁰ The importance of this research is using hydraulic river models combined with the AWBI index to detect surface water. Also, the accuracy of the ABWI index recorded a better value than the NDWI index. Combining optical bands with other indices to identify surface water has shown acceptable results. Jia et al.²⁶ proposed a new extraction surface water body and water inundation mapping method using multi-temporal Landsat 8 data. In this method, they used spectral matching based on discrete particle swarm optimization to demonstrate the water and non-water boundary. Providing lower omission error (OE), removing dark vegetation, and recognizing shadows, ice, and cloud with DEM data makes this method reliable and accurate.²⁶

Synthetic aperture radar (SAR) is used to detect water bodies and flood monitoring whenever optical images cannot penetrate clouds. Bayik et al.²⁷ utilized pre-event and post-event Sentinel-1 images and applied multi-temporal change detection analysis for flood detection in the Meric River to extend flood mapping. To extract water bodies from the Meric River, three approaches, including backscatter thresholding, random forest (RF), and deep learning classification, were used. Their results illustrated that the RF classification was more accurate for surface water

detection than the deep learning method. The overall accuracy (OA) and kappa coefficient for RF were higher than other methods. The important superiority of RF in comparison with other methods is taking less time for classification and being more user friendly than deep learning.²⁷ Amitrano et al.²⁸ used the Sentinel-1 ground range detected images and proposed a new unsupervised method with two processing levels for exploiting rapid flood mapping. They used post-event images for the fuzzy classification system and utilized a change detection index between pre-event and post-event. Results demonstrated that the proposed approaches are more accurate than the other methods. Detection rate (DA) and false alarms (FA) for two proposed chains had better results than the rest.²⁸ Regarding the significance of the research, the ability of Sentinel-1 to detect surface water in any situation was mentioned. Also, using the proposed methods, the classification error has been significantly reduced. Pôssa and Maillard focused on detecting and monitoring small water bodies from Sentinel-1 data in Belo Horizonte, Brazil. They proposed a combination of a support vector machine (SVM) classifier and a marginal water probability map for the distinction of water surfaces from the land. Also, using the probability map derived from SVM classification, the accuracy of water extraction was increased. The obtained results showed that, using the “refined Lee” filter,²⁹ the edges were preserved. Using VV and VV+VH polarization against VH polarization, the accuracy of small water bodies’ extraction was improved.³⁰ It can be seen that, due to the use of Sentinel-1 individually and the supervised classifier (SVM), small water bodies were distinguished with sufficient accuracy. Clement³¹ studied the floods of winter 2015–2016 in Yorkshire using Sentinel-1 data. For flood mapping, a change detection and threshold strategy was used with two processing steps. They provided non-flood reference images for change detection and extracted the inundation extent map with a thresholding method. The VV polarization has provided smother improvement in accuracy compared with VH polarization. Mapped results have a reasonable correlation and high accuracy for flood mapping.³¹ In this study, the Sentinel-1 sensor feature in data collection to prepare an inundation extent map in turbulent weather conditions has been mentioned.

Recently, some research studies have focused on data fusion from different sensors to improve object extraction. Each sensor has unique characteristics by which their fusion provides more details for classification. The combination of sensors made up for some defects such as speckle noise on SAR data and environmental noises (shadow, forest, built-up areas, snow, and clouds) on optical data.^{32–34}

Seaton et al.³⁵ investigated proper water indices to map and monitor changes of water surface areas of non-perennial rivers in semi-arid environments using Sentinel-2 and Landsat-8. They examined NDWI, MNDWI, NDVI, AWEIsh, AWEInsh, and multi-band water index on two satellites to determine the most suitable method. In the classification task, the NDWI from Sentinel-2 top of atmospheric (TOA) reflectance datasets was illustrated to be a suitable index for extracting surface water. Eventually, using multiple moderate-resolution datasets and water indices, the changes of surface water in non-perennial rivers were identified with an easy and accurate method.³⁵ Zoka et al.³⁶ used a fusion of Landsat-7 and Sentinel-1 data for monitoring flood events and their effects in West Thessaly (central Greece). In this method, they applied several indices such as MNDWI, the tasseled cap transformation, the difference between vegetation and water index, and the red and short-wave infrared index (RSWIR) on Landsat-7 and implemented a threshold approach for Sentinel-1 VV polarization data. Since the optical images are unable to penetrate clouds, the results demonstrated that RADAR data improved the accuracy of classification during the flood event. Furthermore, water indices (MNDWI and RSWIR) significantly increased the water body delineation’s accuracy for the flooded area.³⁶

This study tries to fuse MS sensors data and SAR data to extract surface water bodies using an approach based on water indices, supervised classifications, and decision fusion. The decision fusion is used to improve the accuracy of surface water extraction. Water indices and combinations of them are utilized to distinguish between water and non-water; the supervised classification methods such as SVM, neural network (NN), and RF are applied to improve the accuracy of classification. Finally, a decision fusion technique is applied to fuse the achieved results of all three classifiers.

2 Proposed Multispectral and RADAR Data Fusion for Water Body Extraction

This paper introduces a remote sensing multisensor fusion approach based on the fusion of optical and RADAR data for surface water extraction. Figure 1 depicts the general structure of the proposed methodology. This figure shows that two types of remote sensing sensors, including optical (Landsat-8 and Sentinel-2) and RADAR (Sentinel-1) sensors, are utilized to provide complementary information with sufficient details.

The proposed method described in this paper consists of two strategies of data fusion and decision fusion. In the data fusion approach, a combination of optical and RADAR data is applied as the input of the water index mapping and classification model. Then the machine learning classifiers (SVM, NN, and RF) are applied to process the fused data. Finally, in the decision fusion part, all classification results are fused to provide a more accurate classification map. Fusion at the decision-making level is regarded as the highest level of data fusion. At this level of fusion, the obtained decisions are fused using the weighted majority voting (WMV) algorithm. Since each classifier produces different results based on its specific features, the simultaneous use of a set of classifiers enhances the classification results.

2.1 Pansharpening

To achieve the image with high spatial resolution and maintain the spectral data, a pansharpening approach is used. In this study, to increase the spatial resolution from 15 to 10 m for Landsat-8 multispectral image (MSI), Gram–Schmidt (GS), one of the pansharpening operations, fuses this data with Sentinel-2 panchromatic band. The Sentinel-2 panchromatic band is achieved from the mean of RGB bands wavelength. The GS³⁷ algorithm is one of the methods of fusing MSIs. In this algorithm, the panchromatic band is first simulated using MS bands and is fused with other bands.

A GS conversion is applied to the MSIs, as much as the number of fused bands, and the component is created. In the next step, by replacing the first component of this image with the main panchromatic band, the fusion is performed.

Assuming that the set $S = \{v_1, v_2, v_3, \dots, v_n\}$ is the orthogonal basis vectors of the internal multiplication space V , each vector $w \in V$ is represented as a linear combination of the base vectors S .^{38–41}

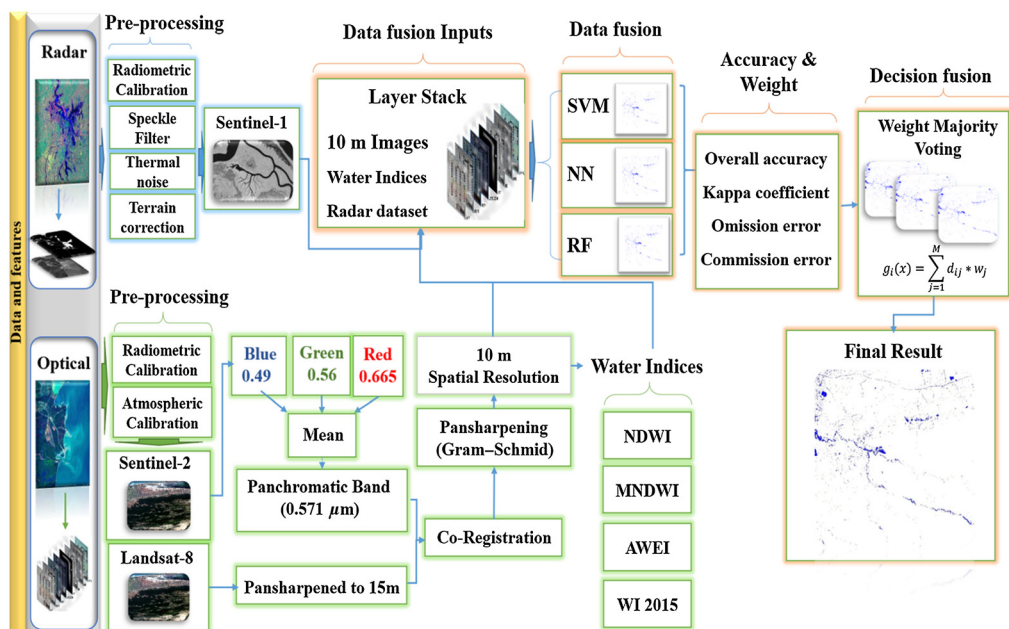


Fig. 1 Proposed remote sensing data fusion for surface water extraction.

$$w = \frac{(w, v_1)}{\|v_1\|^2} v_1 + \frac{(w, v_2)}{\|v_2\|^2} v_2 + \dots + \frac{(w, v_n)}{\|v_n\|^2} v_n, \quad (1)$$

if it is assumed that $\{u_1, u_2, \dots, u_n\}$ is the desired base in the interior internal multiplication space V , then using the GS algorithm orthogonal base, $\{v_1, v_2, \dots, v_n\}$ is formed:

$$\text{Pr } obj_v(u) = \frac{(u, v)}{\|v\|^2} v. \quad (2)$$

- First step

$$v_1 = u_1. \quad (3)$$

- Second step

$$v_2 = u_2 - \text{Pr } obj_{v_1}(u_2). \quad (4)$$

- Third step

$$v_3 = u_3 - \text{Pr } obj_{v_1}(u_3) - \text{Pr } obj_{v_2}(u_3). \quad (5)$$

- N step

$$v_n = u_n - \sum_{j=1}^{n-1} \text{Pr } obj_{v_j}(u_n). \quad (6)$$

In this case, the vector $\{v_1, v_2, \dots, v_n\}$ consisting of n independent linear vectors is formed as the orthogonal base of this space.⁴²

2.2 Water Indices

The water indices are the most useful and straightforward methods for enhancing the differences between water and non-water, which contains two or more spectral bands of sensors that implement algebraic operations.

2.2.1 NDWI

NDWI is the famous water index proposed by McFeeters⁴³ for extracting water from other objects. The near-infrared band with $0.86 \mu\text{m}$ and the green band with $0.56 \mu\text{m}$ are used for vegetation and weak liquid water absorption. NDWI is defined as

$$\text{NDWI} = \{\rho(0.86 \mu\text{m}) - \rho(1.24 \mu\text{m})\} / \{\rho(0.86 \mu\text{m}) + \rho(1.24 \mu\text{m})\}, \quad (7)$$

$$\text{NDWI} = \{(\text{Green} - \text{NIR}) / (\text{Green} + \text{NIR})\}, \quad (8)$$

where $\rho(\lambda)$ is the apparent reflectance and λ is the wavelength. $\rho(\lambda)$ is obtained from

$$\pi L(\lambda) / [\cos(\theta_0) E_0(\lambda)], \quad (9)$$

where $L(\lambda)$ is the measured radiance, θ_0 is the solar zenith angle, and $E_0(\lambda)$ is the solar irradiance above the Earth's atmosphere.⁴⁴ This index has less sensitivity to atmospheric scattering effects, but it cannot distinguish the soil reflectance effects. Consequently, the results are an overestimation of water bodies in urban areas.⁴⁵

2.2.2 MNDWI

MNDWI was proposed by Xu⁴⁶ to enhance the surface water bodies by reducing and even removing built-up land noise as well as vegetation and soil noise, which makes it more suitable for extracting surface water. In this method, the MNDWI utilized the short-wave infrared (SWIR1) band instead of NDWI, which used the NIR band. Using a zero threshold value can efficiently improve the accuracy of water extraction and reveal more details of surface water.

$$\text{MNDWI} = \{(\text{Green} - \text{SWIR1}) / (\text{Green} + \text{SWIR1})\}. \quad (10)$$

2.2.3 AWEI

The automatic water extraction index (AWEI) was proposed by Feyisa et al.⁶ to extract surface water bodies. This index improves surface water extraction accuracy by increasing the spectral difference between water and non-water. Since the thresholding enhances the extraction accuracy, coefficients are used in this formulation to stabilize the threshold. An iterative process based on an experimental study on reflectance patterns is applied on a pure water pixel dataset to determine the coefficients. AWEI improves the accuracy of water extraction for an area in which shadow and dark surface are the main issues. This index is also used for change detection studies since it has stable thresholding and accurately classifies the edge pixel.

- AWEI_sh is used to eliminate shadows or other dark surfaces effectively.

$$\text{AWEI}_{\text{sh}} = \rho_{\text{blue}} + 2.5 \times \rho_{\text{green}} - 1.5 \times (\rho_{\text{NIR}} - \rho_{\text{SWIR1}}) - 0.25 \times \rho_{\text{SWIR2}}. \quad (11)$$

- AWEI_nsh proposed for areas where shadows are not important issues.

$$\text{AWEI}_{\text{nsh}} = 4 \times (\rho_{\text{blue}} - \rho_{\text{NIR}}) - (0.25 \times \rho_{\text{red}} + 2.75 \times \rho_{\text{SWIR2}}). \quad (12)$$

2.2.4 WI₂₀₁₅

This water index was proposed by Fisher et al.;⁴⁷ it was developed in the same way as the WI 2006⁴⁸ and is based on data normalized surface reflectance rather than TOA. WI₂₀₁₅ would be more accurate compared with WI₂₀₀₆ at extracting surface water bodies. They used the optimum threshold and surface reflectance images to provide accurate water extraction methods across large regions. Using linear discriminant analysis classification, values for the coefficients are determined.

$$\text{WI}_{2015} = 1.7204 + 171\rho_{\text{Green}} + 3\rho_{\text{Red}} - 70\rho_{\text{NIR}} - 45\rho_{\text{SWIR1}} - 71\rho_{\text{SWIR2}}. \quad (13)$$

The accuracy of water extraction depends on the size and shape of water bodies. Clear-deep surface water pixels and green-brown water pixels are two classes in which detection of the boundary between them is most difficult. An optimized threshold must be selected to enhance the accuracy of classification. The WI₂₀₁₅ is one of the most accurate indices for surface water extraction.

2.3 Classification Methods

In the classification phase, the proposed method utilized three conventional classification methods including SVM, NN, and RF for the classification of surface water.

2.3.1 Support vector machine

SVM is a machine learning method with associated supervised learning algorithms that analyze data used for classification and regression analysis. This is one of the new methods that has shown good performance in recent years compared with older methods for classification. The basis of the SVM classifier is the linear classification of the data, and in the linear division

of data, it attempts to select the line with the greatest safety margin. SVM classification finds a linear separation that maximizes the boundary of classes and uses a kernel system to transform the data into a higher-dimensional space.

$$f(x) \sum_{i=1}^L \alpha_i y_i k(x_i, x_j) + \gamma. \quad (14)$$

According to Eq. (14), α_i is the Lagrange multiplier variables, y is used to move the hyperplane by the threshold variable, and the kernel function is defined as $k(x_i, x_j)$.^{49,50} This paper applied an radial basis function kernel for the SVM classifier.⁵¹

$$k(x, x') = \exp(-\lambda \|x - x'\|^2). \quad (15)$$

Here, feature vectors are defined by x and x' and K and λ are the kernel function and kernel variable, respectively. A comprehensive search using a grid search is performed to set the SVM kernel parameters with the best result; then a set of appropriate parameter values are provided. In this type of classification, a grid search method is applied to select the SVM classifier.

2.3.2 Neural network

The NN is a novel computational system for machine learning, knowledge display, and finally applied knowledge acquisition to maximize the output response of complex systems. A vital element of this idea is the creation of new structures for the information processing system. This approach consists of a large number of highly interconnected processing elements called neurons that work together to solve a problem and transmit information through synapses. The learning in these systems is adaptive, meaning that, using examples, the weight of the synapses is altered in such a way that the new system produces the correct response. One of the most common methods of solving the optimization problem is backpropagation NNs.^{52,53}

$$a_c = \sum_p w_{pc} \times b_{pc}. \quad (16)$$

In Eq. (16), a_c is the sum of the multiplications of inputs by their weight, w_{pc} is the weight of this input, and (b_{pc}) contains the value of neurons c , which inputs from neurons p . If the data are denoted with $(x_1, y_1), \dots, (x_n, y_n)$ and the cost function with l , the goal is to achieve the following function:

$$Q(W) = \sum_{i=1}^n l(h_w(x_i), y_i), \quad (17)$$

where x_i s the input, y is the output, and NN output is $h_w(x)$.

2.3.3 Random forest

The RF is widely used for classification and regression; it works based on a structure consisting of a large number of decision trees, training time, and classification results. RFs are suitable for decision trees that are overfitting in the training set. Various methods of machine-learning use decision trees as a standard method for different applications. To tree learn, the training algorithm applies the general technique of bootstrap aggregating or bagging. Datasets are shown with D , $D = (x_1, y_1), (x_2, y_2), \dots, (x_n, y_n)$, bagging regularly (B times) selects a random sample with replacement of the training set and fits trees to these samples. The final model works by averaging or voting between trees. In the regression problem, the final model is the mean of all trees:

$$\hat{f} = \frac{1}{B} \sum_{b=1}^B f_b(x'). \quad (18)$$

In the classification problem, the final answer is obtained by voting between the trees. The above procedure describes the original bagging algorithm for trees.⁵⁴

As a result, the RF classifier is widely utilized to classify the dataset. One of RF's benefits is the power of handling large datasets with higher dimensionality. It can handle thousands of input variables and identify the most significant variables, so it is considered one of the dimensionality reduction methods. Further, the results can be combined with other decision-making techniques to achieve better results.⁵⁵ The discrimination function is specified as

$$H(x) = \arg \max_y \sum_{i=1}^k I(h_i(X, \theta_k) = Y), \quad (19)$$

where the classifier $h(x, \theta_k)$: (θ_k) is a random vector, X is an input vector, $I(\cdot)$ is the index function, $h(\cdot)$ is defined as the decision tree, the variable output is determined by Y , and “ $\arg \max_y$ ” denotes the value of Y when Eq. (20) is maximized.⁵⁴

$$\sum_{i=1}^k I(h_i(X, \theta_k) = Y). \quad (20)$$

2.4 Decision Fusion

Decision fusion, or more generally, the fusion of data, combines or fuses different decisions from different methods or data to finally make a more accurate and trustworthy decision compared with the result of an individual decision. One of the most important and widely used methods in decision fusion is a method based on the concept of voting,⁵⁶ wherein each decision-making method is considered an individual vote. The simplest form of this method is maximum voting. In this method, if all decision-making methods have the same weight and accuracy, all classifiers' decisions for an input sample are considered with the same weight, and the decision with the highest vote is introduced as the winner class for that specific sample input. In a simple voting method in which the weight of all classifiers is equal, the class with the maximum number of votes wins [Eq. (21)].

$$\sum_{i=1}^L d_{i,k} = \max_{j=1}^L d_{i,j}. \quad (21)$$

In Eq. (21), d_i , $i = 1, \dots, m$ (where m is the number of sets of decision methods), $j = 1, \dots, c$, (where c is the number of classes available), and the c -dimension vector $\{d_{i1}, d_{i2}, \dots, d_{in}\}$ can be considered for each classifier. The $d_{i,j}$ value can be 0 or 1 when the decision method assumes the input sample to be included in or excluded from the particular class in question.⁵⁷ When the classifiers have different weights, a specific model of this method called WMV is used. In this way, the role of more accurate classifiers in voting increases, and they are given more weight, while less accurate classifiers receive less weight in the fusion.

$$g_i(x) = \sum_{j=1}^M d_{ij} * w_j. \quad (22)$$

In Eq. (22), w_j is the weight of each classifier and is determined using the OA assessment.

3 Dataset and Study Area

The proposed method was performed using multisensor data, including MS Sentinel-2, Landsat-8, and RADAR Sentinel-1 datasets, which have a different spatial resolution of 20, 30, and 10 m, respectively.

The Landsat-8 satellite provides free MS data for global monitoring using two OLI and Thermal Infrared Sensor sensors with 11 bands that contain 10 bands with 30 m spatial

Table 1 Information of Landsat 8, Sentinel-2, and Sentinel-1.

Satellite	Sensor type	Spatial resolution (m)	Number of bands	Acquisition date
Landsat-8	Optical	30	11	June 6, 2019
Sentinel-2	Optical	20	12	June 4, 2019
Sentinel-1	RADAR	10	2	June 3, 2019

resolution and one band (panchromatic) with 15 m.⁵⁸ Also, Sentinel-2 is an Earth observation project developed by the European Space Agency as part of the Copernicus Program to improve Earth observation missions and support services such as forest monitoring, land cover change management, and natural disaster management. The project includes two identical Sentinel-2A and Sentinel-2B satellites with 13 spectral bands, with four bands at 10 m, six bands at 20 m, and three bands at 60 m spatial resolution.⁵⁹ Furthermore, Sentinel-1 performs imaging on a RADAR basis and can collect and capture phenomena regardless of the effects, such as imaging during the day or at night and in various weather conditions.⁶⁰ Table 1 illustrates the Sentinel-2 and Landsat-8 details, such as the number of bands, color bands, and spatial resolution.

Neka and its adjacent areas were considered the two study areas. Neka is the city and capital of Neka County, Mazandaran Province, Iran. Mazandaran province with latitude 36.5656°N 53.0588°E, with an area of 23,833 km², constitutes 1.5% of Iran's territory. Two regions were studied in Mazandaran province, each having complex environmental conditions such as forest, surface water, agricultural land, rivers, and wasteland. Therefore, it is vital to monitor and detect surface water in these two areas.

The first study area (Gelevard Dam) (Fig. 2) covers an area of 420 km² with specific environmental effects. In this study, the rivers leading to the dam were examined using data fusion and decision fusion strategies.

The second study area (Fig. 3) includes Neka city, Mazandaran Province. The most important factors in choosing this area for study are buildings, forests, and muddy rivers. In addition, the Neka River, which crosses the city center, has a history of frequent floods. This area covers an area of 420 km², similar to the first area.

In addition, 52,347 training pixels for the first study area and 40,138 training pixels for the second study area are defined and assigned. Finally, to evaluate and obtain the confusion matrix, 76,136 test pixels for the first study area and 108,059 test pixels for the second study area are utilized.

4 Experiments and Results

In experimental results, two strategies are applied to detect surface water. In the first, the data fusion consists of 10 m spatial resolution images, water indices, and RADAR datasets. The second is the fusion of three classifier results using a WMV approach called decision fusion.

In this paper, data fusion included the combination and fusion of MSIs (pansharpened to 10 m spatial resolution), RADAR dataset, and water indices in one layer. The dataset was processed by supervised classifiers (SVM, NN, and RF) for water extraction.

Using radiometric and atmospheric correction for Landsat-8 MSIs, the dataset is ready for pansharpening to 15 m. The Landsat-8 panchromatic band with the GS algorithm allows the spatial resolution to increase from 30 to 15 m. After increasing the spatial resolution to 15 m, by obtaining the panchromatic band from the mean of the red, green, and blue wavelength (0.571 μm) of the Sentinel-2 satellite, spatial resolution was increased to 10 m by the GS method, which is depicted in Fig. 4.

Additionally, the RADAR dataset is stacked with all extracted spectral features to increase the accuracy of the water extraction strategy. The final data contain 14 bands, including seven bands of Landsat-8, two VV and VH images of Sentinel-1 RADAR data, and five water indices

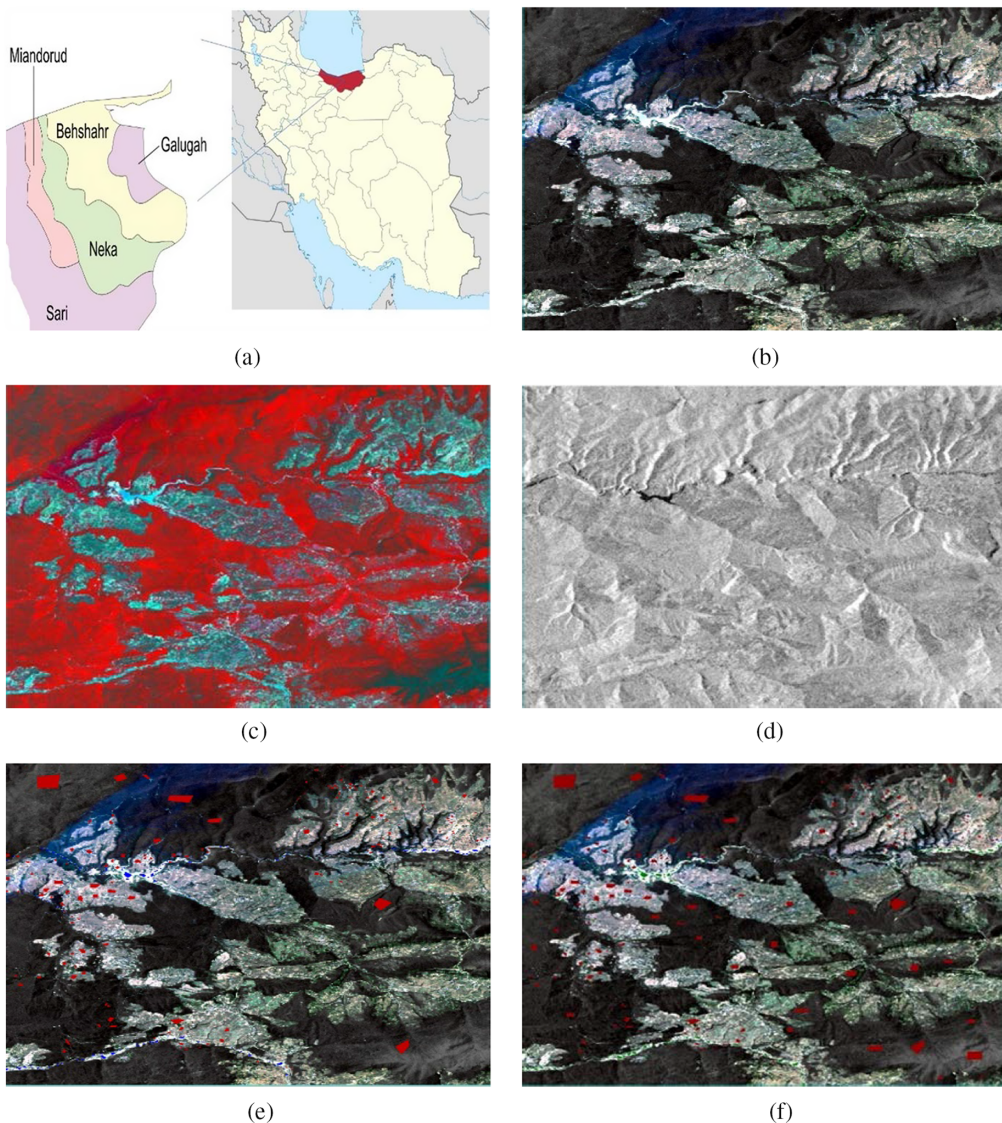


Fig. 2 The first study area (Gelevard Dam): (a) Mazandaran Province, Iran, (b) RGB visible bands of the first study area (true color), (c) false-color map, (d) Sentinel-1 dataset to illustrate water from non-water, (e) train data for the supervised classifier (red = non-water, green = water), and (f) test data for assessments of accuracy (red = non-water, blue = water).

(NDWI, MNDWI, AWEI_sh, AWEI_nsh, and WI2015). Figures 5 and 6 depict the extracted features from the datasets of study areas, such as water indices and the Sentinel-2 panchromatic band.

The machine learning method substantially improved surface water extraction from the complex environment. Due to the accuracy of machine learning strategies, three powerful supervised classifiers, including SVM, NN, and RF, are utilized to extract water from the surface with acceptable accuracy. Figures 7 and 8 show the surface water extraction for three classifiers, SVM, NN, and RF for the two study areas.

To increase the accuracy of surface water extracted by three classifiers (SVM, NN, and RF), a decision fusion strategy is used to integrate the output images using WMV method; it significantly increase the accuracy of the final result.

These classifiers are implemented on a data fusion strategy for the two study areas. Table 1 and Fig. 9 show the fusion strategy results based on data fusion and decision fusion systems. Also, the WMV method is utilized as a decision fusion based on the voting strategy. The decision fusion results demonstrate that WMV provides higher OA and kappa coefficient (k) values.

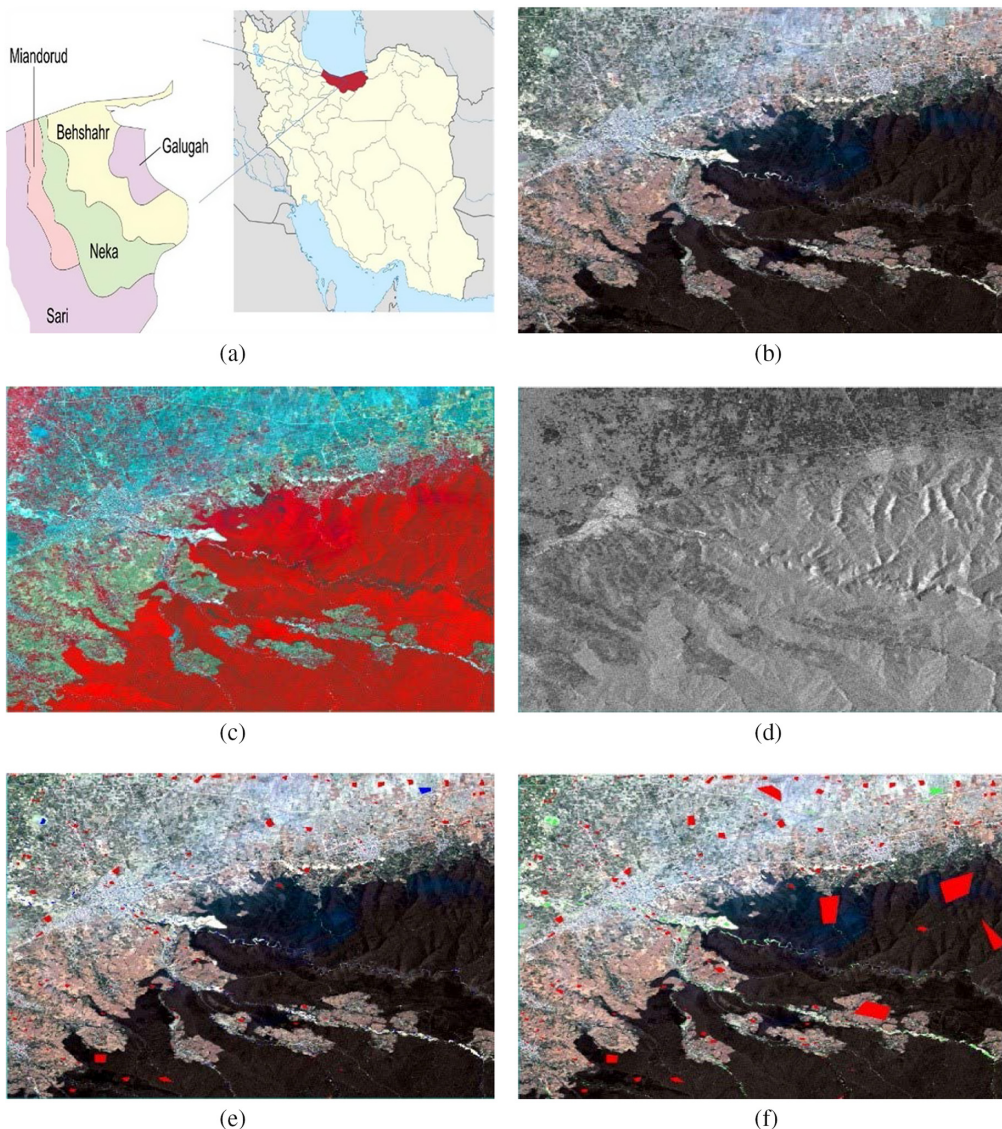


Fig. 3 The second study area (Neka city): (a) Neka city, Mazandaran Province, Iran, (b) RGB visible band of second study area (true color), (c) false-color map, (d) Sentinel-1 dataset to illustrate water from non-water, (e) train data for the supervised classifier (red = non-water, green = water), and (f) test data for assessments of accuracy (red = non-water, blue = water).

Table 2 shows a comparison between the data and the decision fusion strategy. The results depict that WMV as decision fusion provides better accuracy than the traditional classifiers (SVM, NN, and RF). Moreover, it can be observed that, based on the data fusion strategy, the RF is more accurate than the other two classifiers (SVM and NN) in surface water extraction. As can be seen, the study area is located in the north of Iran. In this region, agricultural land, where rice is grown, is irrigated by small rivers most days of the year, which is one reason for identifying more water. On the other hand, in most articles, the RF classifier is more accurate in identifying surface water than the other classifiers.²⁷ The accuracy of this supervised classifier is indicated in Table 2.

The RF classifier has an OA of 96.87% and a kappa coefficient (k) of 0.8541 for the first study area and OA of 96.73% and a kappa coefficient (k) of 0.8389 for the second study area. Using the WMV method, the OA and kappa coefficient enhanced to 98.86% and 0.8965 for the first study area and 98.56% and 0.8941 for the second study area, respectively. As seen, the proposed decision fusion strategy represents the best accuracy with a growth in an OA that

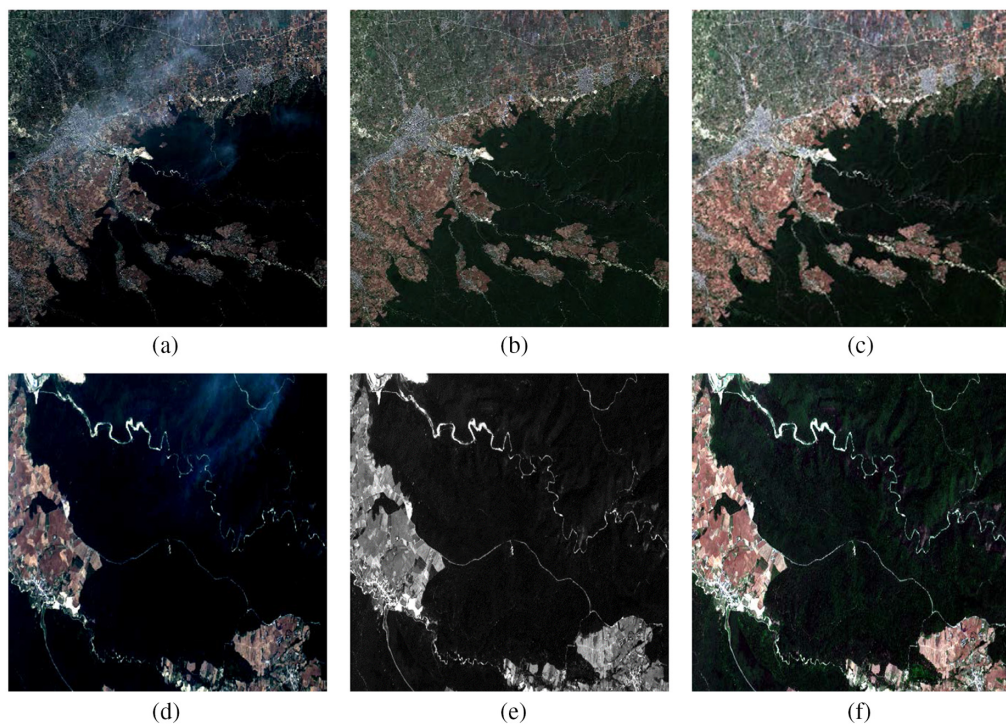


Fig. 4 The pansharpened images of Landsat-8, Sentinel-2, and fusion of Landsat-8 with Sentinel-2. (a) Landsat-8 pansharpened to 15 m, (b) Sentinel-2 panchromatic band 10 m, (c) fusion of the Landsat-8 and Sentinel-2 that pansharpened to 10 m, (d) crop of Landsat-8 pansharpened to 15 m, (e) crop of Sentinel-2 panchromatic band 10 m, and (f) crop of fusion of the Landsat-8 and Sentinel-2 that pansharpened to 10 m.

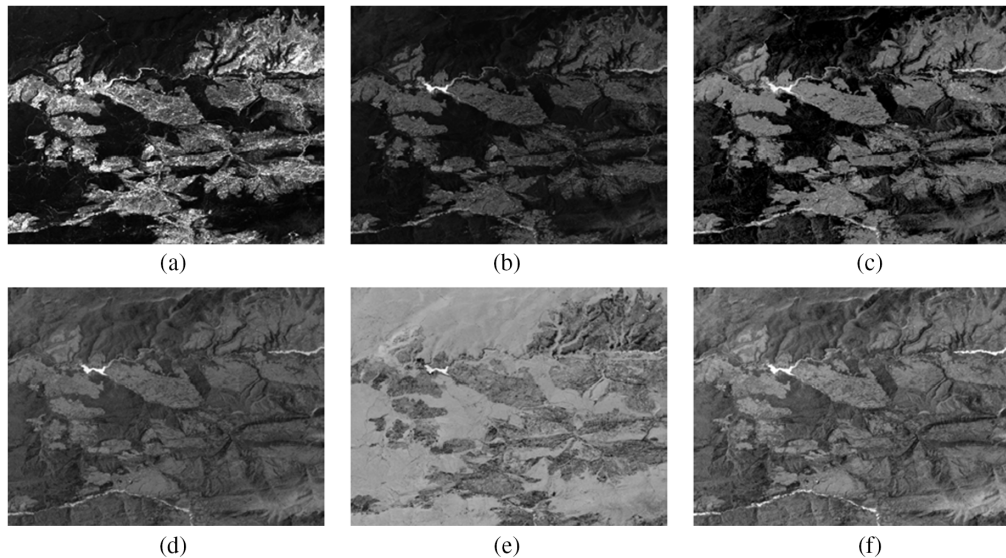


Fig. 5 All features of the first study area. (a) Sentinel-2 panchromatic band ($0.571 \mu\text{m}$), (b) NDWI, (c) MNDWI, (d) AWEI_{sh}, (e) AWEI_{nsh}, and (f) WI2015

improves the accuracy of data fusion up to 1.99% and 1.83% for the first and the second study areas, respectively.

To validate the proposed method, which included the fusion of two types of sensors (Landsat-8 and Sentinel-2) to achieve a quality of 10 m, Landsat-8 and Sentinel-2 pansharpened images were used with SVM, NN, and RF classifiers to extract surface water. The results are given in

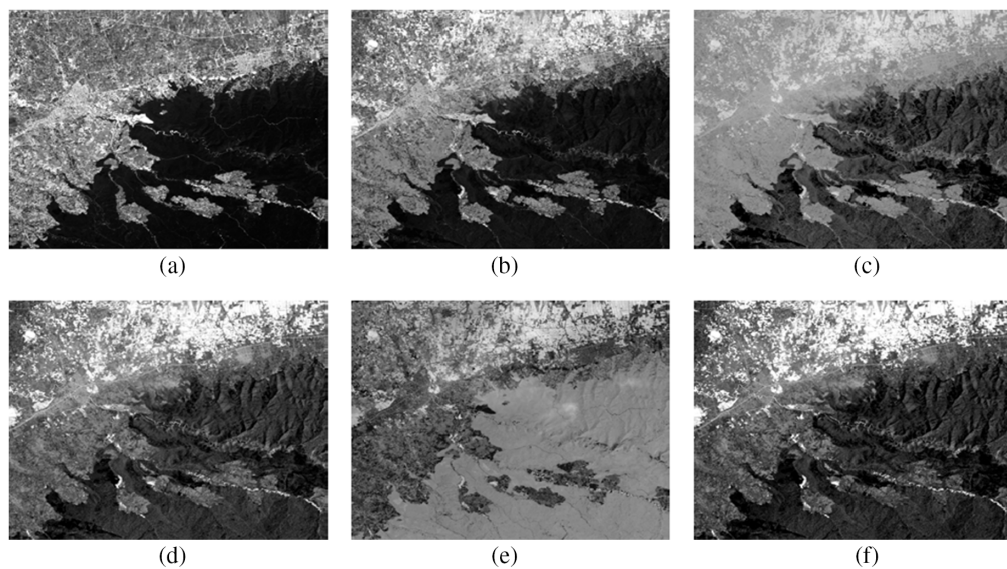


Fig. 6 All features of the first study area. (a) Sentinel-2 panchromatic band ($0.571 \mu\text{m}$), (b) NDWI, (c) MNDWI, (d) AWEI_sh, (e) AWEI_nsh, and (f) WI2015.

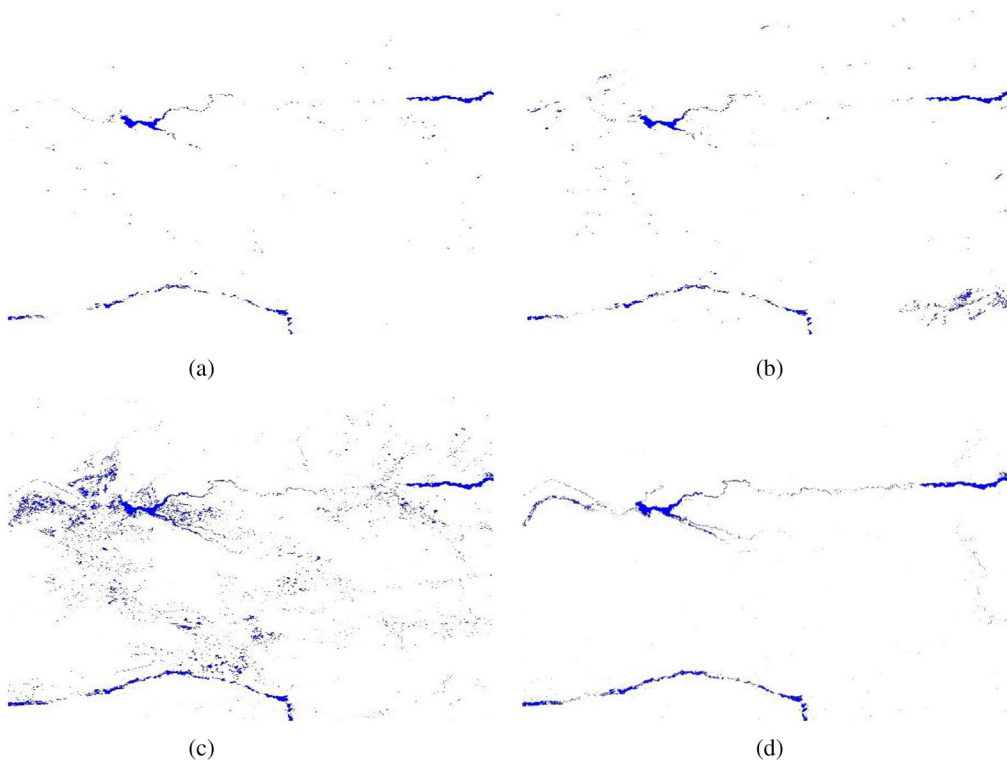


Fig. 7 Results of the machine learning method for the first study area. (a) SVM, (b) NN, (c) RF, and (d) WMV.

Tables 3 and 4, which depict that, in the best scenario, the RF classifier for Landsat-8 and Sentinel-2 for the first study area has an 11.76% and 5.57% lower OA, respectively, and for the second study area, the difference is 8.8% and 6.59%, respectively.

To compare the accuracy of five other combinations, including

- combination of 10 m MSI with RADAR data,
- MSI combined with water indices,

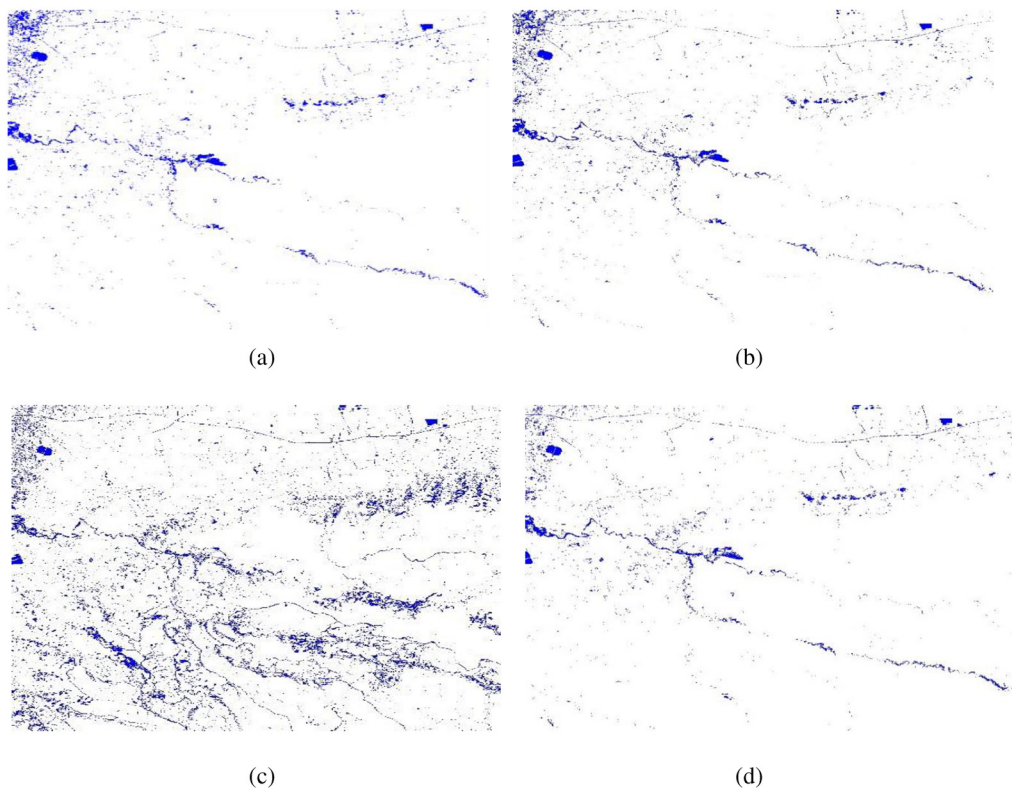


Fig. 8 Results of the machine learning method for the second study area. (a) SVM, (b) NN, (c) RF, and (d) WMV.

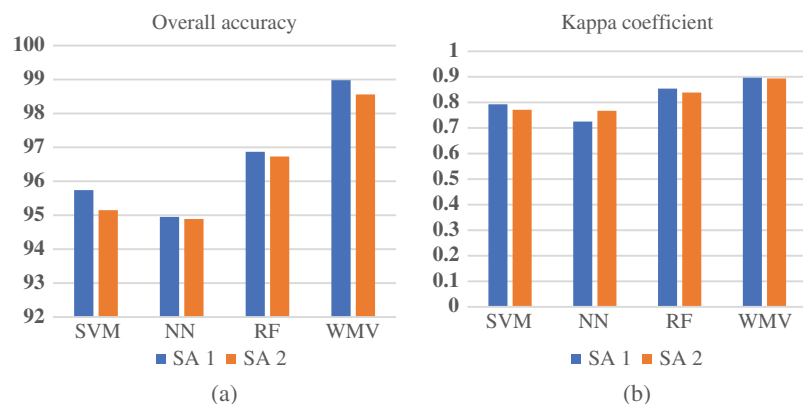


Fig. 9 Data fusion and decision fusion OA and kappa (k) accuracy. (a) OA of study areas and (b) kappa coefficient of study areas.

Table 2 Accuracy assessment of the data fusion approach for the two study areas.

Classifier		SVM	NN	RF	WMV
Study area 1 (Gelvard Dam)	OA	95.74%	94.95%	96.87%	98.86%
	K	0.7929	0.7254	0.8541	0.8965
Study area 2 (Neka city)	OA	95.15%	94.89%	96.73%	98.56%
	K	0.7714	0.7672	0.8389	0.8941

Table 3 Comparison of the results of classification for other satellites with the GS algorithm pan-sharpening method for the first study area.

Study area 1 classifier		SVM	NN	RF
Landsat-8 (15 m spatial resolution)	OA	79.54%	76.94%	85.11%
	K	0.6111	0.5823	0.6487
Sentinel-2 (10 m spatial resolution)	OA	89.21%	88.17%	91.3%
	K	0.6475	0.6109	0.7086
Data fusion Landsat-8 + Sentinel-2 (10 m spatial resolution)	OA	95.74%	94.95%	96.87%
	K	0.7929	0.7254	0.8541

Table 4 Comparison of the results of classification for other satellites with the GS algorithm pan-sharpening method for the second study area.

Study area 2 classifier		SVM	NN	RF
Landsat-8 (15 m spatial resolution)	OA	78.52%	77.02%	87.93%
	K	0.609	0.57	0.6629
Sentinel-2 (10 m spatial resolution)	OA	88.67%	86.81%	90.14%
	K	0.6159	0.601	0.6892
Data fusion Landsat-8 + Sentinel-2 (10 m spatial resolution)	OA	95.15%	94.89%	96.73%
	K	0.7714	0.7672	0.8389

- MSI bands,
- indices, and
- RADAR data,

three SVM, NN, and RF classifiers were applied. The results of the classifier show that the accuracy of other combinations is lower than the proposed combination.

Figure 10 shows that the OA and kappa coefficient were calculated for all proposed methods and all three classifiers for the two study areas.

Table 5 represents the commission error and OE of classifiers and the decision fusion approach. Based on these results, decision fusion decreases the error of independent classifiers' results. It can be seen that the decision fusion strategy illustrated the lowest error in the first study area, with a commission error of 0.1768 and 0.0011 for water and land (non-water), respectively. The results also indicated WMV's superiority over supervised classifiers in the OE for water and land (non-water) with 0.0203 and 0.0176, respectively. Furthermore, in the second study area, the commission error was 0.1027 and 0.0193 for water and land (non-water), respectively, and the OE for water and land (non-water) was 0.0252 and 0.0074, respectively.

A review of the results for both study areas shows that using a data fusion strategy increased the spatial resolution of the MS bands to 10 m. With this approach, there were more pixels for classification, which provided sufficient and appropriate accuracy. Then, to improve the results achieved, a decision fusion strategy was used to combine all of the results of the classifiers (SVM, NN, and RF) with the WMV approach. The results of the proposed method were more accurate than the results of the classifiers.

Tables 5 and 6 illustrate the accuracies of the two study areas to show the comparisons between the proposed methods and other combinations, which are classified by SVM, NN, and RF. It can be seen that water indices, in combination with the MSI layer, increased the kappa

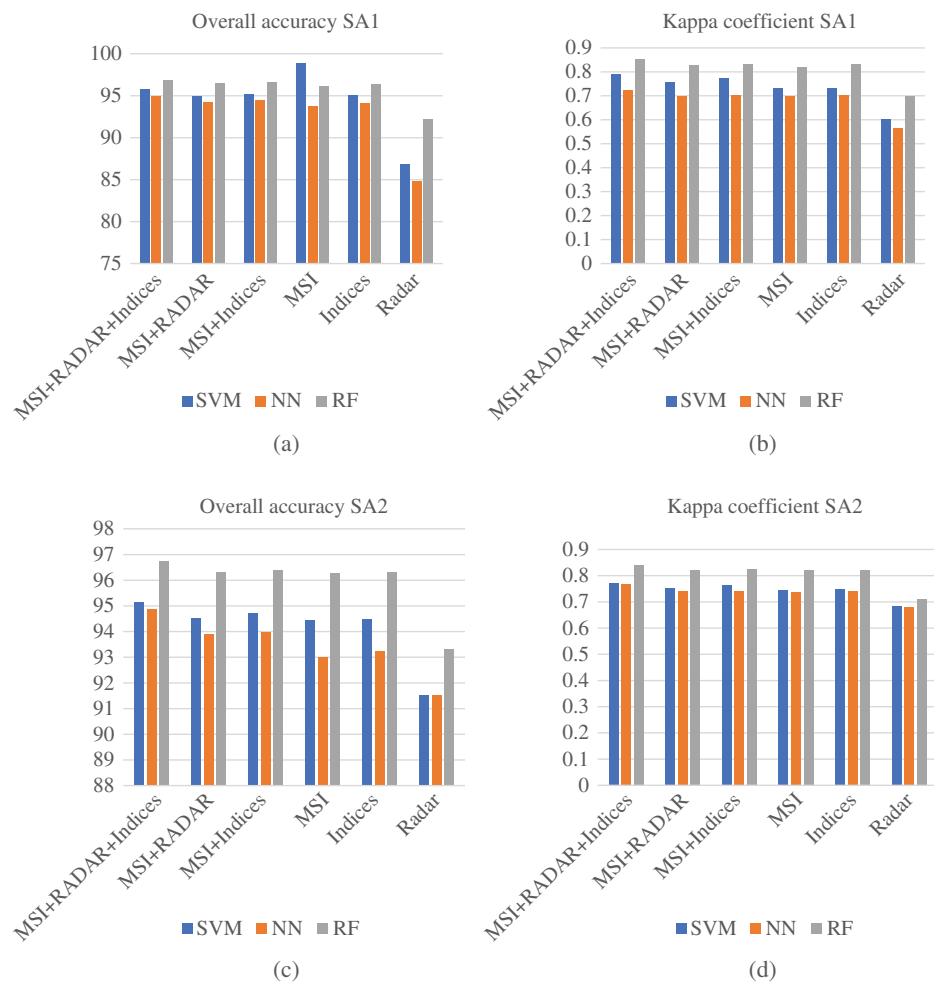


Fig. 10 Study areas OA and the kappa coefficient. (a) The first study area OA of all combinations. (b) The first study area kappa coefficient of all combinations. (c) The second study area OA of all combinations. (d) The second study area kappa coefficient of all combinations.

Table 5 Commission error and OE of the data fusion approach for the two study areas.

Classifier		SVM		NN		RF		WMV	
		Land	Water	Land	Water	Land	Water	Land	Water
First study area	Commission	0.0031	0.3258	0.0041	0.3303	0.002	0.2043	0.0011	0.1768
	Omission	0.0472	0.0371	0.0490	0.0386	0.0289	0.0350	0.0176	0.0203
Second study area	Commission	0.0108	0.4414	0.0127	0.4978	0.083	0.1849	0.0193	0.1027
	Omission	0.0498	0.0941	0.0576	0.1638	0.0194	0.0683	0.0074	0.0252

coefficient as well as the OA for both study areas, which has a significant role in identifying surface water. The results show that RADAR images enhance the accuracy of classifiers in water and non-water detection (Table 7).

5 Discussions and Conclusions

Currently, environmental changes are a critical threat to human survival, water, and food resources. Water has great importance as a primary and vital need to survive humanity and satisfy its

Table 6 OA and kappa of other combination for the first study area.

		MSI + RADAR + indices	MSI + RADAR	MSI + indices	MSI	Indices	RADAR
SVM	OA	95.74%	94.91%	95.17%	98.86%	95.02%	86.84%
	K	0.7929	0.7562	0.7731	0.7331	0.7357	0.6025
NN	OA	94.95%	94.23%	94.52%	93.79%	94.11%	84.84%
	K	0.7254	0.6978	0.7015	0.6998	0.7015	0.5639
RF	OA	96.87%	96.53%	96.59%	96.19%	96.41%	92.19%
	K	0.8541	0.8291	0.8314	0.8221	0.8338	0.6973

Table 7 OA and kappa of other combination for the second study area.

		MSI + RADAR + indices	MSI + RADAR	MSI + indices	MSI	Indices	RADAR
SVM	OA	95.15%	94.53%	94.73%	94.46%	94.50%	91.51%
	K	0.7714	0.751	0.7621	0.7461	0.7501	0.6852
NN	OA	94.89%	93.91%	93.98%	93.00%	93.24%	91.21%
	K	0.7672	0.7416	0.7429	0.7371	0.7397	0.6792
RF	OA	96.73%	96.31%	96.38%	96.2%	96.31%	93.30%
	K	0.8389	0.822	0.8241	0.8198	0.8219	0.711

requirements. As one of the most available resources in nature, surface water can fulfill this need to a large extent. Also, by detecting and monitoring surface water, risks such as floods and droughts can be prevented.

In this study, we have proposed identifying and extracting surface water using two data fusion and decision fusion strategies. As shown in Table 1, the decision fusion approach uses the WMV method to integrate data fusion output data. The result is accompanied by an increase in OA and kappa coefficient.

The principal contributions of the proposed methodology are as follows:

- Surface water bodies have a vital role in our lives; therefore, detecting and monitoring surface water to satisfy human necessities and regional decisions are important.
- For extraction of surface water bodies, optical and RADAR sensors both were used because they fix each other's defects, such as cloudy weather, low light conditions, and the distinction between textures.
- To increase the spatial resolution to identify low-width surface waters, the fusion of optical sensor data could increase spatial resolution accuracy from 30 to 10 m. The resulting data provided an image with a spatial resolution quality of 10 m and preserved the spectral properties at an acceptable quality.
- A combination of water indices can improve accuracy in identifying surface water by enhancing the distinction between water and non-water. In this paper, NDWI, MNDWI, AWEI, and WI are used to distinguish water from non-water. Also, water indices have an effective role in enhancing surface water detection using machine learning methods.
- Using water indices and pansharpened images can improve low-resolution images' ability to enhance surface water detection accuracy with low, wide rivers or turbid water.

- Machine learning methods have higher accuracy and speed in classifying classes due to their ability to learn based on training data. Supervise classifiers (SVM, NN, and RF) in the data fusion approach, extracted the surface water more accurately.
- The fusion of different classifier results can produce a better understanding of the observed site. The decision fusion approach can enhance classification accuracy by combining the classification algorithms' results on different datasets compared with a single classifier.
- The classifiers' results are fused with the WMV method based on the decision fusion strategy, which decreases the omission and commission errors and detects more surface water accurately.

The results show that, with the decision fusion strategy using the WMV method, the accuracy of the extracted surface water increases to an acceptable value. It allows us to achieve an adequate level of accuracy compared with other methods.

Consequently, this research proposed data fusion and decision fusion strategies with innovations to detect surface water more accurately. These innovations consist of the following:

- The fusion of two optical sensors to use the details of spectral data of both sensors instead of using a single sensor to increase the separation of spatial resolution to 10 m.
- The dataset consists of water indices to differentiate between water and non-water, RADAR data to increase water identification accuracy, and 10 m of MSI for edge extraction.
- The classifiers' results are integrated using the WMV method to increase surface water detection accuracy.
- It can be said that the decision fusion approach has been able to easily improve the accuracy of surface water identification as much as possible by reducing the errors of classifiers in distinguishing between water and non-water.

References

1. K. Alderman, L. R. Turner, and S. Tong, "Floods and human health: a systematic review," *Environ. Int.* **47**, 37–47 (2012).
2. N. R. Bond, P. S. Lake, and A. H. Arthington, "The impacts of drought on freshwater ecosystems: an Australian perspective," *Hydrobiologia*, **600**, 3–16 (2008).
3. F. Sun et al., "Comparison and improvement of methods for identifying waterbodies in remotely sensed imagery," *Int. J. Remote Sens.* **33**, 6854–6875 (2012).
4. A. Karpatne et al., "Global monitoring of inland water dynamics: state-of-the-art, challenges, and opportunities," in *Computational Sustainability*, J. Lassig, K. Kersting, and K. Morik, Eds., pp. 121–147, Springer (2016).
5. C. Huang et al., "Detecting, extracting, and monitoring surface water from space using optical sensors: a review," *Rev. Geophys.* **56**(2), 333–360 (2018).
6. G. L. Feyisa et al., "Automated water extraction index: a new technique for surface water mapping using Landsat imagery," *Remote Sens. Environ.* **140**, 23–35 (2014).
7. C. Giardino et al., "Application of remote sensing in water resource management: the case study of Lake Trasimeno, Italy," *Water Resour. Manage.* **24**, 3885–3899 (2010).
8. T. D. Acharya et al., "Classification of surface water using machine learning methods from Landsat data in Nepal," in *Proc. Int. Electron. Conf. Sens. and Appl.*, Vol. 4, No. 1, p. 43 (2018).
9. B. C. Naik and B. Anuradha, "Extraction of water-body area from high-resolution Landsat imagery," *Int. J. Electr. Comput. Eng.* **8**(6), 4111 (2018).
10. L. Xiong et al., "Subpixel surface water extraction (SSWE) using Landsat 8 OLI data," *Water* **10**(5), 653 (2018).
11. B. Bigdeli and P. Pahlavani, "A Dempster Shafer-based fuzzy multisensor fusion system using airborne lidar and hyperspectral imagery," *Int. J. Remote Sens.* **39**(21), 7718–7737 (2018).
12. P. A. Brivio et al., "Integration of remote sensing data and GIS for accurate mapping of flooded areas," *Int. J. Remote Sens.* **23**(3), 429–441 (2002).

13. E. Psomiadis, "Flash flood area mapping utilising SENTINEL-1 radar data," *Proc. SPIE* **10005**, 100051G (2016).
14. V. Tsyganskaya et al., "SAR-based detection of flooded vegetation—a review of characteristics and approaches," *Int. J. Remote Sens.* **39**(8), 2255–2293 (2018).
15. A. Twele et al., "Sentinel-1-based flood mapping: a fully automated processing chain," *Int. J. Remote Sens.* **37**(13), 2990–3004 (2016).
16. G. J.-P. Schumann and D. K. Moller, "Microwave remote sensing of flood inundation," *Phys. Chem. Earth, Parts A/B/C* **83**, 84–95 (2015).
17. S. Long, T. E. Fatooyinbo, and F. Policelli, "Flood extent mapping for Namibia using change detection and thresholding with SAR," *Environ. Res. Lett.* **9**(3), 35002 (2014).
18. A. Refice et al., "SAR and InSAR for flood monitoring: examples with COSMO-SkyMed data," *IEEE J. Sel. Top. Appl. Earth Obs. Remote Sens.* **7**(7), 2711–2722 (2014).
19. G. Simone et al., "Image fusion techniques for remote sensing applications," *Inf. Fusion* **3**(1), 3–15 (2002).
20. B. Bigdeli, H. Amini Amirkolaei, and P. Pahlavani, "Deep feature learning versus shallow feature learning systems for joint use of airborne thermal hyperspectral and visible remote sensing data," *Int. J. Remote Sens.* **40**(18), 7048–7070 (2019).
21. T. D. Acharya et al., "Combining water indices for water and background threshold in Landsat image," in *Proc. Int. Electron. Conf. Sens. and Appl.*, Vol. 2, No. 3, p. 143 (2017).
22. T. D. Acharya, A. Subedi, and D. H. Lee, "Evaluation of water indices for surface water extraction in a Landsat 8 scene of Nepal," *Sensors (Switzerland)* **18**(8), 2580 (2018).
23. N. Otsu, "A threshold selection method from gray-level histograms," *IEEE Trans. Syst. Man Cybern.* **9**(1), 62–66 (1979).
24. W. Jiang et al., "A new index for identifying water body from SENTINEL-2 satellite remote sensing imagery," *ISPRS Ann. Photogramm. Remote Sens. Spatial Inf. Sci.* **3**, 33–38 (2020).
25. M. I. Ali et al., "Detection of changes in surface water bodies urban area with NDWI and MNDWI methods," *Int. J. Adv. Sci. Eng. Inf. Technol.* **9**(3), 946–951 (2019).
26. K. Jia et al., "Spectral matching based on discrete particle swarm optimization: a new method for terrestrial water body extraction using multi-temporal Landsat 8 images," *Remote Sens. Environ.* **209**, 1–18 (2018).
27. C. Bayik et al., "Exploiting multi-temporal Sentinel-1 SAR data for flood extend mapping," *Int. Arch. Photogramm. Remote Sens. Spatial Inf. Sci.* **XLII**, 18–21 (2018).
28. D. Amitrano et al., "Unsupervised rapid flood mapping using," *IEEE Trans. Geosci. Remote Sens.* **56**(6), 3290–3299 (2018).
29. J.-S. Lee, "Refined filtering of image noise using local statistics," *Comput. Graphics Image Process.* **15**(4), 380–389 (1981).
30. E. M. Pôssa and P. Maillard, "Precise delineation of small water bodies from Sentinel-1 data using support vector machine classification," *Can. J. Remote Sens.* **44**(3), 179–190 (2018).
31. M. A. Clement, "Multi-temporal synthetic aperture Radar flood mapping using change detection," *J. Flood Risk Manage.* **11**, 152–168 (2017).
32. G. Kaplan and U. Avdan, "Sentinel-1 and Sentinel-2 data fusion for wetlands mapping: Balikdami, Turkey," *Int. Arch. Photogramm. Remote Sens. Spatial Inf. Sci.* **XLII-3**, 729–734 (2018).
33. Q. Wang et al., "Fusion of Landsat 8 OLI and Sentinel-2 MSI data," *IEEE Trans. Geosci. Remote Sens.* **55**(7), 3885–3899 (2017).
34. N. Clerici et al., "Fusion of Sentinel-1A and Sentinel-2A data for land cover mapping: a case study in the lower study in the lower Magdalena region, Colombia," *J. Maps* **13**, 718–726 (2017).
35. D. Seaton, T. Dube, and D. Mazvimavi, "Use of multi-temporal satellite data for monitoring pool surface areas occurring in non-perennial rivers in semi-arid environments of the Western Cape, South Africa," *ISPRS J. Photogramm. Remote Sens.* **167**, 375–384 (2020).
36. M. Zoka, E. Psomiadis, and N. Dercas, "The complementary use of optical and SAR data in monitoring flood events and their effects," *Proceedings* **2**, 1–8 (2018).

37. Q. Wang et al., "Remote sensing of environment fusion of Sentinel-2 images," *Remote Sens. Environ.* **187**, 241–252 (2016).
38. W. Cheney, *Linear Algebra: Theory and Applications*, 2nd ed., Jones & Bartlett Learning
39. L. N. Trefethen and D. Bau III, *Numerical Linear Algebra*, Vol. 50, SIAM (1997).
40. G. H. Golub and C. F. vanLoan, *Matrix Computations*, The Johns Hopkins (1996).
41. C. E. Soliverez and E. R. Gagliano, "Orthonormalization on the plane: a geometric approach," *Rev. Mex. Fís.* **31**(4), 743–758 (1984).
42. L. Pursell and S. Y. Trimble, "Gram–Schmidt orthogonalization by Gauss elimination," *Am. Math. Mon.* **98**(6), 544–549 (1991).
43. S. K. McFeeters, "The use of the normalized difference water index (NDWI) in the delineation of open water features," *Int. J. Remote Sens.* **17**(7), 1425–1432 (1996).
44. B. Gao, "NDWI: a normalized difference water index for remote sensing of vegetation liquid water from space," *Remote Sens. Environ.* **58**(3), 257–266 (1996).
45. X. Huang et al., "Combining pixel-and object-based machine learning for identification of water-body types from urban high-resolution remote-sensing imagery," *IEEE J. Sel. Top. Appl. Earth Obs. Remote Sens.* **8**(5), 2097–2110 (2015).
46. H.-Q. Xu, "A study on information extraction of water body with the modified normalized difference water index (MNDWI)," *J. Remote Sens.* **5**, 589–595 (2005).
47. A. Fisher, N. Flood, and T. Danaher, "Comparing Landsat water index methods for automated water classification in eastern Australia," *Remote Sens. Environ.* **175**, 167–182 (2016).
48. T. Danaher and L. Collett, "Development, optimisation and multi-temporal application of a simple Landsat based water index," in *Proc. 13th Aust. Remote Sens. and Photogramm. Conf.*, Canberra, Australia. Vol. 29 (2006).
49. C. J. C. Burges, "A tutorial on support vector machines for pattern recognition," *Data Mining Knowl. Discov.* **2**(2), 121–167 (1998).
50. B. Schölkopf and A. Smola, "Support vector machines and kernel algorithms," in *Encyclopedia of Biostatistics*, P. Armitage and T. Colton, Eds., pp. 5328–5335, Wiley (2005).
51. F. Imbault and K. Lebart, "A stochastic optimization approach for parameter tuning of support vector machines," in *Proc. 17th Int. Conf. Pattern Recognit., 2004. ICPR 2004.*, IEEE, Vol 4, pp. 597–600 (2004).
52. M. A. Nielsen, *Neural Networks and Deep Learning*, Vol. 2018, Determination Press, San Francisco, California (2015).
53. G.-B. Huang, Q.-Y. Zhu, and C.-K. Siew, "Extreme learning machine: theory and applications," *Neurocomputing* **70**(1–3), 489–501 (2006).
54. L. Breiman, "Random forests," *Mach Learn.* **45**(1), 5–32 (2001).
55. L. Breiman et al., *Classification and Regression Trees*, Taylor & Francis (1984).
56. L. I. Kuncheva et al., "Limits on the majority vote accuracy in classifier fusion," *Pattern Anal. Appl.* **6**(1), 22–31 (2003).
57. D. Ruta and B. Gabrys, "An overview of classifier fusion methods," *Comput. Inf. Syst.* **7**(1), 1–10 (2000).
58. "Landsat-8 satellite," https://www.usgs.gov/land-resources/nli/landsat/landsat-8?qt-science_support_page_related_con=0#qt-science_support_page_related_con.
59. "Sentinel-2 satellite," <https://sentinel.esa.int/web/sentinel/missions/sentinel-2>.
60. "Sentinel-1 satellite," <https://sentinel.esa.int/web/sentinel/missions/sentinel-1>.

Mostafa Saghafi received his BSc degree in civil engineering from Gonabad University in 2018. He is a student working toward his MSc degree in water and hydraulic structures at Shahrood University of Technology. His main interests are in data fusion of multispectral and radar data, data and decision fusion methods, water and flood detection, and the application of Python in remote sensing.

Ahmad Ahmadi received his BSc degree from Ferdowsi University in 1988 and his MSc degree in civil engineering from Tabriz University in 1991. After 6 years as an academic staff member at Shahrood University of Technology, he moved to the UK and started his research studies at

Imperial College, London. He received his PhD in civil engineering hydraulics in 2002. He has been working as an associate professor in the Civil Engineering Department at Shahrood University of Technology since 2005. His main interests are in two-phase air and water flows and fluid-structure interaction.

Behnaz Bigdeli received her BSc degree in geomatics engineering from KNT University in 2007 and her MSc degree in photogrammetry from Tehran University in 2010. She started her PhD research in 2010 and received her PhD in 2014. Since 2020, she has been working at Shahrood University of Technology as an assistant professor. Her main interests are in data fusion of space-borne and airborne data, hyperspectral and lidar processing, decision fusion methods, application of remote sensing, and machine learning in water and environment.